Egyptian Journal of Petroleum (2016) xxx, xxx–xxx

HOSTED BY

ELSEVIER

Egyptian Petroleum Research Institute

Egyptian Journal of Petroleum

www.elsevier.com/locate/egyjp
www.sciencedirect.com

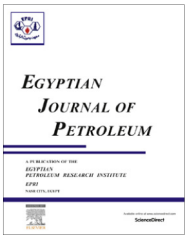

FULL LENGTH ARTICLE

Geophysical investigation in the Northwestern part of the Gulf of Suez, Egypt

Sultan Awad Sultan Araffa [a,*], **Adel M.E. Mohamed** [a,b], **Fernando M. Santos** [c]

[a] *National Research Institute of Astronomy and Geophysics (NRIAG), Helwan, Cairo, Egypt*
[b] *Earthquake Monitoring Center (EMC), Sultan Qaboos University (SQU), Oman*
[c] *IDL – University of Lisbon, Lisbon, Portugal*

Received 7 March 2016; revised 21 June 2016; accepted 29 June 2016

KEYWORDS

3-D VES inversion;
Seismic refraction;
Fault elements;
Fresh and salt water

Abstract Vertical Electrical Soundings (VES) and shallow seismic refraction data interpretation have been used to delineate groundwater aquifer and fault elements which are dissecting the northwestern part of Gulf of Suez. Thirty-five Vertical Electrical Soundings (VES) were carried out and inverted through 3-D VES inversion to determine the subsurface stratigraphy, structures and groundwater aquifer potentialities. The results of VES inversion indicate that the study area consists of four geoelectrical units interpreted as surficial dry sand and gravels deposits, underlain by fresh water bearing zone, salt water bearing unit and limestone layer, at the bottom. The 3-D VES inversion indicates that the area is dissected by normal fault of NE-SW direction. Thirty-four shallow seismic refraction profiles of 94 m spread length have been used to delineate the geotechnical characteristics of surface layers, subsurface structures and subsurface lithology. The results of shallow seismic refraction indicate that the shallow part of the subsurface section consists of three layers, the first soil layer (dry gravels and sands of the recent deposits) underlain by the second soil layer (sands and gravels of the Pleistocene) while the third layer is the bedrock layer of sandstone and shale belonging to the Middle Miocene.

1. Introduction

The study area lies near the shore line of the Gulf of Suez, occupying an area of 548,000 m^2 in the northwestern part of the Gulf of Suez. It is bounded by latitudes 29° 44′ 10″ – 29° 44′ 20″N and longitudes 32° 21′ 30″ – 32° 22′ 20″E. It lies near two roads, the first is the Cairo-Sokhna road and the second is the Suez-Sokhna paved road along the Gulf of Suez coast and is surrounded by many mountains such as Ataqa Mountain, Kaheilyia Mountain, Abou Treifiya Mountain, Akheider Mountain and El Galala El Bahariya plateau. The main wadis near the study area are streaming into the coastal plain and the Gulf of Suez. These Wadis are, from north to south, Wadi Hagoul, Wadi Beda, Wadi Akheider, Wadi Hammamat and Wadi Ghuweiba (Fig. 1). Many authors have carried out valuable geological, geophysical and structural works around the study area as [1–8].

* Corresponding author.

Peer review under responsibility of Egyptian Petroleum Research Institute.

http://dx.doi.org/10.1016/j.ejpe.2016.06.002

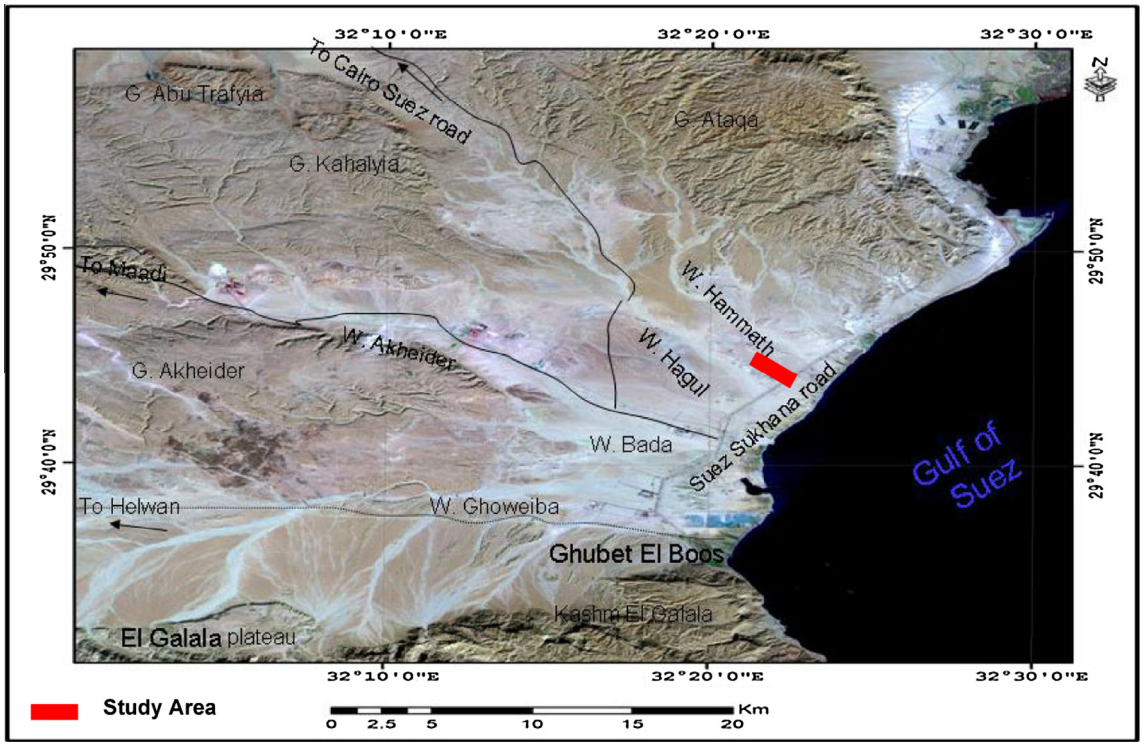

Figure 1 Location map of the study area.

Several algorithms have been developed to perform 3-D resistivity modeling and inversion. 3-D forward algorithms based on the finite-difference, finite-element and integral methods have been presented by several authors [9–14], just to refer to some of the papers published in the last decade. 3-D VES inversion can be used to distinguish between the various rock units and structures at different depth levels. [15] used 3-D VES inversion to delineate structural as well as some geological parameters at Cairo-Ismailia desert road. [16] applied 3-D VES inversion with gravity and magnetic interpretation to delineate groundwater occurrences and structural elements at Insha area near Cairo. [17] applied integrated interpretation of geological, geoelectrical, shallow seismic and geotechnical data to delineate the subsurface stratigraphy and structures at May15th City located in south Cairo. [18] delineated the structural elements around Greater Cairo using gravity and magnetic data. In the present work, we used the results of 3-D VES and shallow seismic refraction data to delineate the fresh groundwater aquifer to be used in developing the industrial area which contains many factories and national projects. Another objective in this study is to delineate the subsurface structural elements (faults) which dissect the area and evaluate the suitable sites for any infrastructural purposes.

2. Geology of the area

Geomorphologically, the study area is characterized by plenty of hills and wadis, which are covered by calcareous boulders and gravels. Their sources are the near and surrounding mountains such as Ataqa Mountain in the north and Kaheilia and Um Zieta Mountains in the northwest. Although El Galala El Bahariya plateau lies in the south of the study area, its effect appears in the drainage form, which descends from the northern face of the plateau. Most of the wadis descend from Ataqa Mountain, Akheider Mountain and El Galala El Bahariya plateau.

The subsurface stratigraphy of the area under investigation is exposed at the surface in two locations around the study area. The first is at Akheider Mountain in the western side of the region and completed by the faulted sections below. The layers of these faulted sections are dipping to the east until they are covered by recent alluvium at the coastal plain. The second location is at Ataqa Mountain, where the old rocks at the low southern margins of Ataqa Mountain and their layers are dipping at this part to the south and southwest. Also the old rocks are exposed on the surface below the series of the western mountains, which include Kaheilia and Um Zieta Mountains with layers dipping toward the eastern and southeastern directions. Fig. 2 shows the geological map of the study area. The surface geology was discussed in [19,20] and the subsurface stratigraphy was described by [21] (Fig. 3). The surface geological map indicates that the study area and its surrounding regions are covered by rock units extending from Middle Eocene to Quaternary deposits. The Middle Eocene rocks (E2) covering the northern part of the area under investigation, exist in two successions, one at Ataqa Mountain area (Ramia Formation) and the other in the western part (Hof Formation). The Middle Eocene rocks are represented by a succession of limestone in Akheider Mountain. Upper Eocene units (E3) are exposed at the low southern margins of Ataqa Mountain and represented by Hof Formation which consists of clay, marl and fossiliferous calcareous sandstone. Middle Miocene (M2) rock units are of shallow marine origin, consisting of a succession of marl, coarse sand and clay, and occupying the greatest part cropped out in the area and correspond to the

Please cite this article in press as: S.A.S. Araffa et al., Geophysical investigation in the Northwestern part of the Gulf of Suez, Egypt, Egypt. J. Petrol. (2016), http://dx.doi.org/10.1016/j.ejpe.2016.06.002

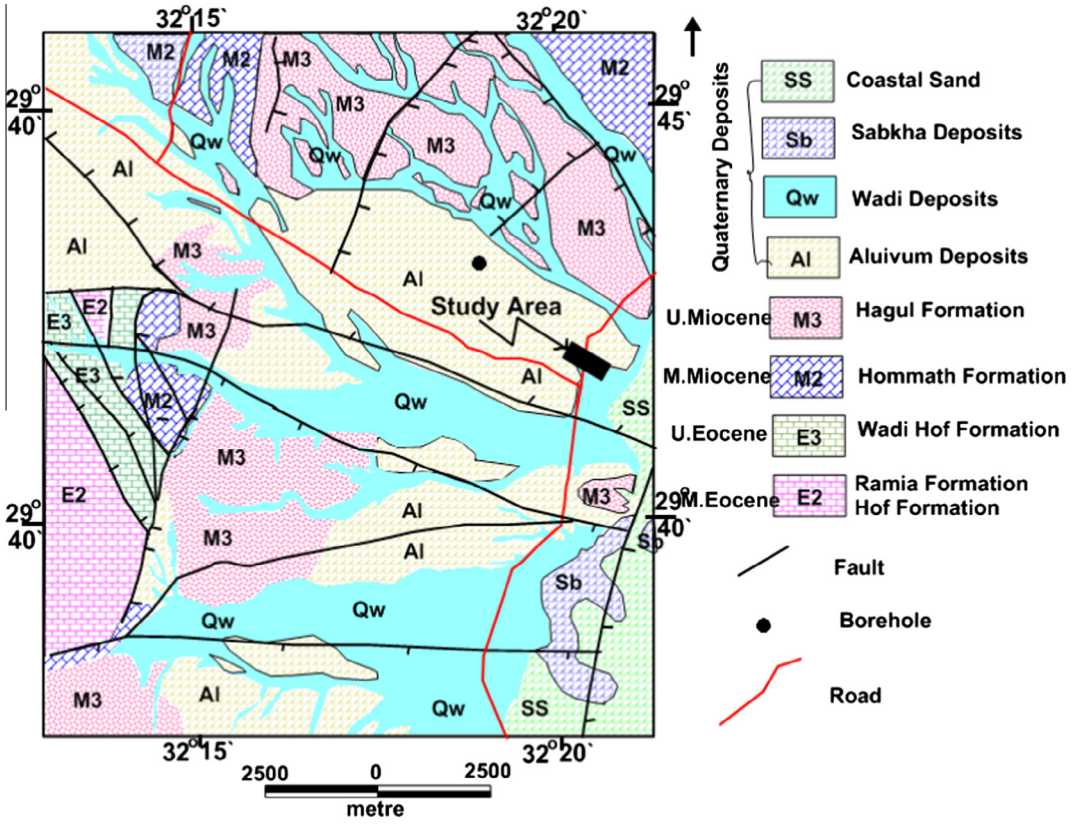

Figure 2 Geological map of the study area (modified after [19]).

Hommath Formation. Upper Miocene (M3) deposits are represented by Hagul Formation which consists of white to yellow calcareous sandstone, with an average thickness of about 24 m. The lower part includes thin layers of green marl. These rocks are found in the plateau, which is raised by 35 m and extends between Wadi Hagul and Wadi El Badaa. Quaternary deposits are represented by the recent deposits, which covered the coastal plain, wadis, and the low areas below the surrounding mountains until reaching the shore line. These deposits include alluvium (AL) which consists of big gravel boulders of limestone mixed with sand and gypsum, and Wadi deposits (QW) consisting of calcareous boulders covering the surface of the wadis near the high mountains (Akheider, El Galala El Bahariya, Ataqa, Kaheilia and Um Zieta Mountains) which vary in thickness and increase toward the eastern direction and reach 25 m at Wadi Ghuweiba. The coarse deposits are covered by mud and silt produced by flash flood, especially near the wadis influx, coastal sand (SS), and Sabkha (SB) where parts of the coastal sands are wet by seawater forming salty deposits. The area under investigation and surrounding regions were dissected by many normal faults; the majority has the NW-SE direction. There is a horst fault system that extends from the northeastern margin of Akheider Mountain, between Wadi El Badaa and Wadi Akheider. There is a normal fault, which cuts the southeastern part of Akheider Mountain parallel to Wadi Ghuweiba and has the trend E-W, where the Middle Eocene layers formed this part of the plateau at high elevations north of the fault in front of the faulted layers of Middle Miocene to the south direction of this normal fault. There is a normal fault intersected by the two faults of the horst system in the northeastern margin of Akheider Mountain and affects the Middle Eocene layers in the plateau itself. In the northwestern part of the studied area, there is a normal fault, which has a NW-SE trend and which extends to a distance about 23 km. Eight kilometers of these faults pass west of Um Zieta Mountain, in addition to 15 km. parallel to the southern margin of Wadi Hagul to the Gulf of Suez direction [20].

3. Methodology

3.1. Geoelectric data

3.1.1. Geoelectric data acquisition

Thirty-five Vertical Electrical Soundings (VES) have been acquired using sensitive resistivity-meter model Syscal-R2 with AB/2 ranging from 1 to 600 m in order to investigate the shallow and deep sections, as well as, to determine the zones of fresh water which overlay the introducing salt and brackish water which is coming from the Gulf of Suez. The VES station locations represent a grid of 165 × 110 m. Those VES stations were performed along four profiles, each profile consisting of 9 VESes except the southern profile which includes 8 VESes as shown in Fig. 4a. Three-to-four-layer models can in general, explain the main features of the curves. Most curves are of the type H, revealing a second conductive layer in the VESes of the survey which corresponds to salt water invading from the Gulf of Suez. The last layer reveals high resistivity corresponds to limestone in the study area. One VES station was

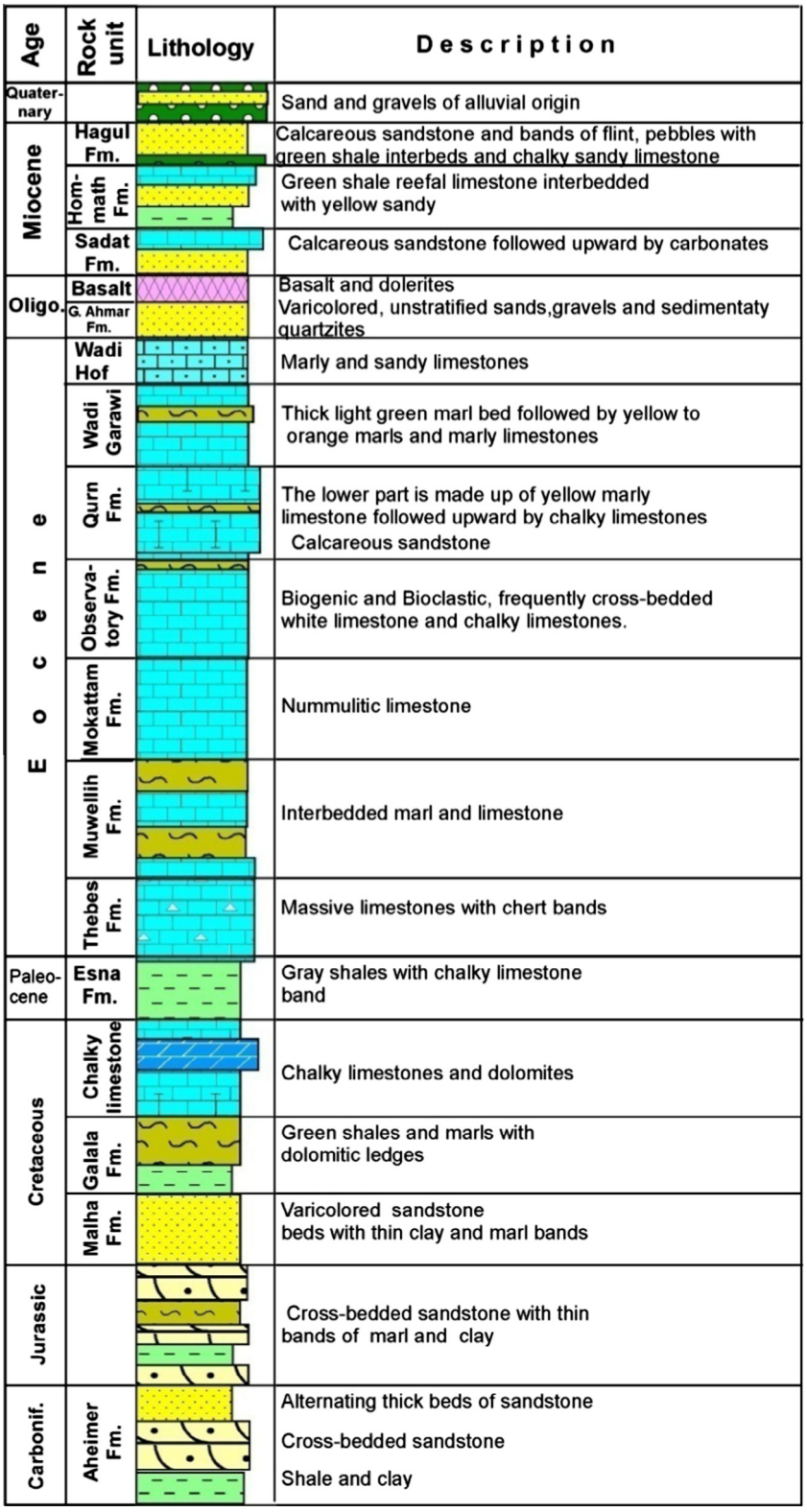

Figure 3 Composite section in the studied area without vertical scale (modified after [21]).

measured at a borehole drilled by [19] at a distance of 2.5 km northwest away from the study area. The results of the drilling report of the borehole indicate that the subsurface consists of Quaternary deposits of sand and gravel of high resistivity that overlay a fresh water aquifer, then salt and brackish water until depth about 100 m. Fresh and salt water aquifer overlay limestone layers until depth of 220 m and exhibits resistivity values about 20 Ohm m (Fig. 5).

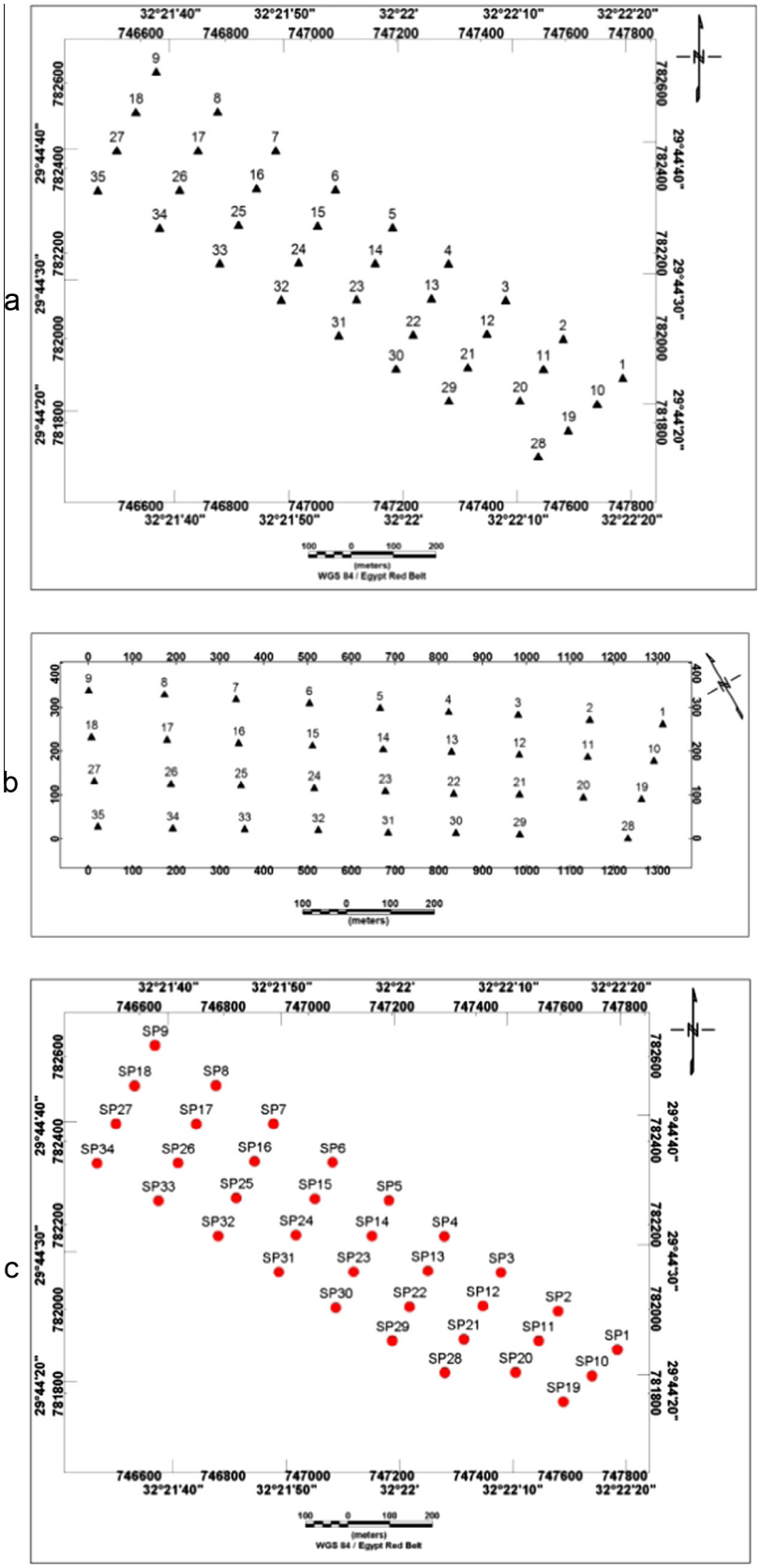

Figure 4 Location map of VES stations, (a) before rotation, (b) after rotating 30 degree anti-clockwise and (c) locations of seismic profiles.

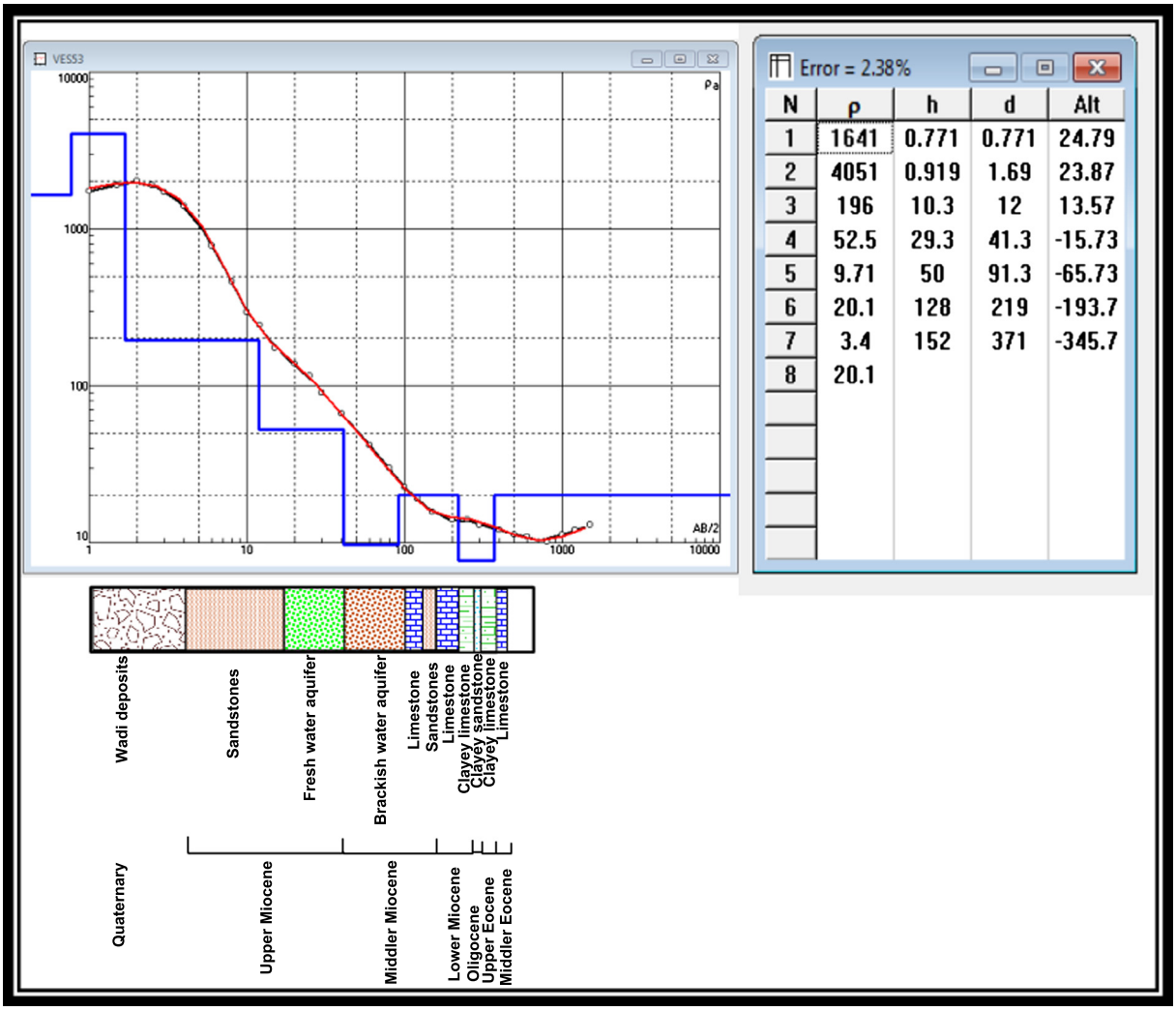

Figure 5 Interpretation of one VES station calibrated with borehole-1 using IPI2WIN program.

3.1.2. 3-D Resistivity interpretation

The 3-D inversion code used in this work was developed using the finite-element approach for forward calculations and a smoothness-constrained least-squares algorithm for inversion [22,23,15]. The program uses an irregular mesh constructed for each VES site, taking into account sounding parameters (AB/2 spacing and azimuths of AB layout of VES arrangements). The area of VES station was rotated 30 degrees to prepare the mesh size of the model (Fig. 4b). The thirty-six VES stations measured in the study area starting with AB/2 = 1 and have a maximum AB/2 of 600 m. Before the data with bearing inverted the VESs of the shallow spacing from AB/2 = 1 to 5 were deleted from all VES to decrease the error of inversion, which, in general, is higher than 5% for short AB/2. All VES data with AB/2 from 6 to 600 m, representing 540 data points, were inverted considering the subsurface domain divided into 1920 hexahedral elements of unknown resistivity. Horizontally, the finite element mesh was defined for each sounding, in general, with 91×96 nodes. A 50 ohm-m (corresponding to the average apparent resistivity data) uniform medium was considered for initial model. The regularization algorithm proposed by [24] was adopted in this work. The results presented in this section have been obtained using a regularization parameter of 0.3, which corresponds to the better fitting between data and model responses. This result was obtained after several inversion runs with different parameters. The program is running for 20 iterations to reach good results. The comparison between measured and calculated apparent resistivity curves is shown in Fig. 6. The misfit between data and model responses varies between soundings: a huge misfit is observed at VES station 23, a high misfit is observed at the longest AB/2 spacing for VESes no.7, 12, 20 and 24. For the majority of the soundings the fit is quite good, with RMS error lower than 10% as shown in Fig. 6.

3.1.3. Horizontal slices for 3-D VES inversion

The horizontal slices have been carried out at different depths such as 2, 5.5, 10, 14, 20.5, 27.5, 35, 70, 90, 125 and 175 m (Fig. 7) where the salt water is revealed by the resistivities lower than 10 Ohm.m (0.1–10 Ohm.m). This salt water filling the aquifer is due to the water invasion from Gulf of Suez.

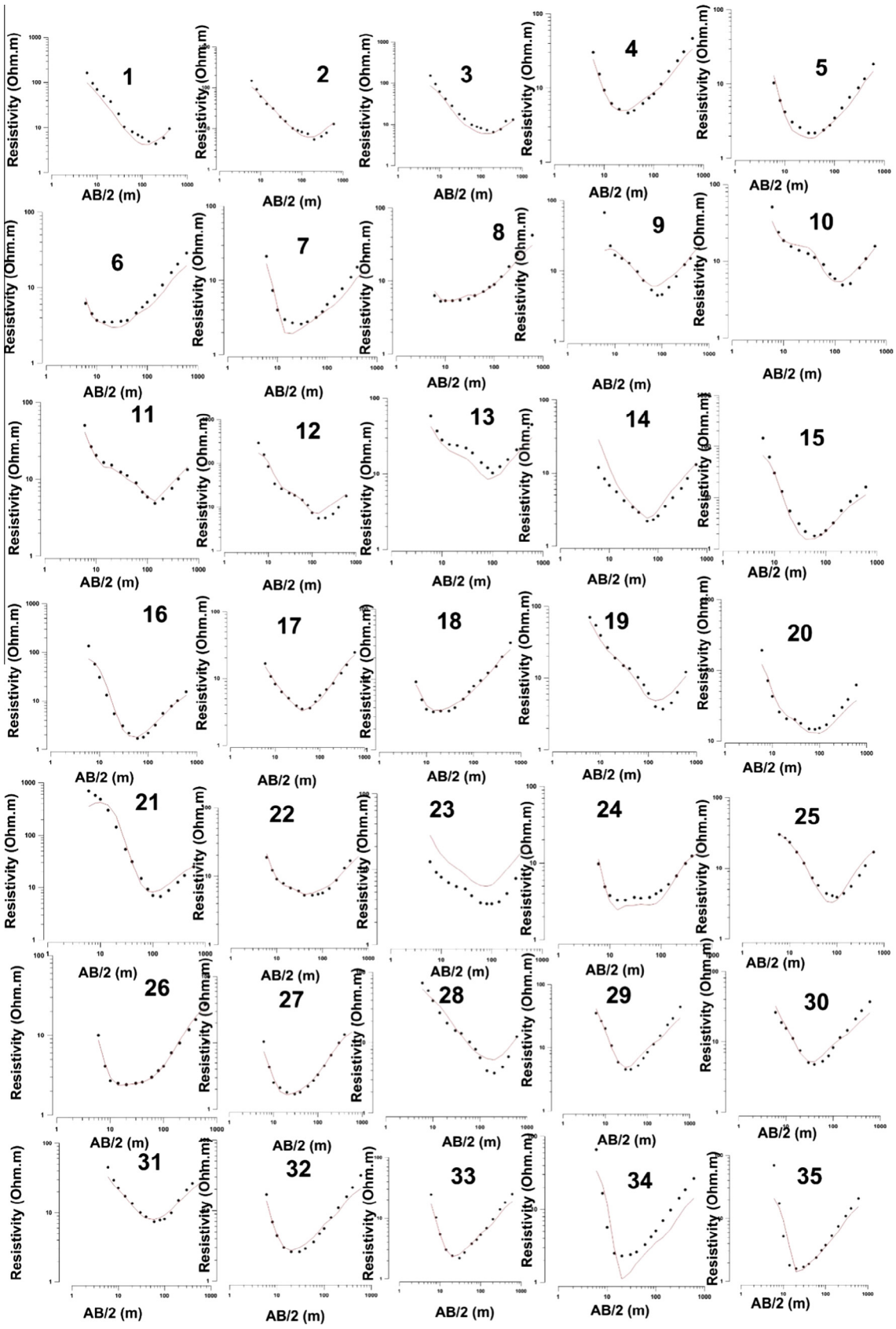

Figure 6 Comparison between observed and calculated resistivity data from 3-D VES inversion.

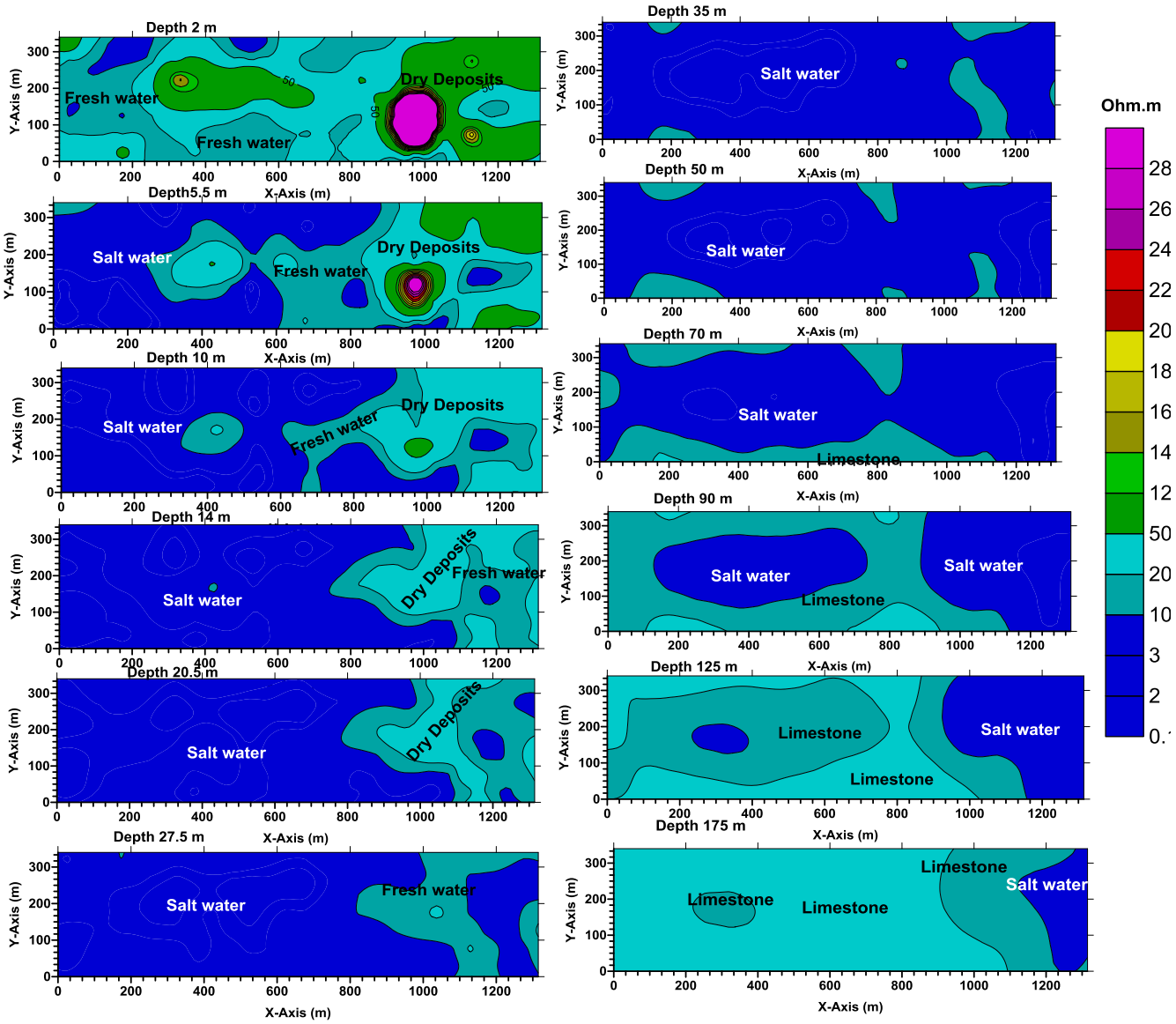

Figure 7 Horizontal slices at different depths as a result of 3D VES inversion.

The salt water at southeastern part of the study area is presented in VES No. 1, 2, 10, 11, 19 and 28 at depths greater than 175 m while in the northwestern part of the area is revealed shallower and appears at a depth of 125 m. This salt water overlays limestone saturated by salt water which shows resistivity values ranging from 20 to 50 Ohm.m. The upper surface of limestone layer is detected at a depth of 50 m and the lower surface is undetected where it is continuous for more than 175 m. The salt water zone is overlain by an aquifer of fresh water, which exhibits resistivity values from 10 to 20 Ohm.m and is detected at depth from 5 to 35 m. This fresh water zone is overlaid by dry deposits of sand and gravels and reveals high resistivity values. The thickness of the dry deposits increases from the northwestern part to the southeastern part (from few meters to 35 m). Fig. 7 indicates that the study area is dissected by a normal fault in the southwestern part passing approximately through the locations of VESes No. 4, 3, 22 and 30.

3.1.4. Vertical slices on Y-axis direction for 3D VES inversion

The vertical slices from the results of 3-D VES inversion have been extracted along *Y*-axis every 50 m, the slice No.1 being at distance of 25 m from the origin of *X*-axis and ending at slice no .7 at distance 325 m along *X*-axis. The sections indicate that the subsurface consists mainly of four geoelectric units, the first unit is sand and gravels at shallow depth with thickness ranging from a few meters in the northwestern part of the sections to about 20.5 m in the southeastern part of sections. The second geoelectric unit represents the fresh water bearing zone, exhibiting resistivity values from 10 to 20 Ohm.m and its depth ranges from 5 to 35 m, overlying the salt water bearing zone. The third geoelectric unit is corresponding to salt water bearing zone which reveals low resistivity values ranging from 0.1 to 10 Ohm.m and its depth extends from a few meters in the northwestern part of the sections to 20 m. The fourth geoelectric unit represents the limestone layer which exhibits high resistivity ranging from 20 to 50 Ohm.m (Fig. 8).

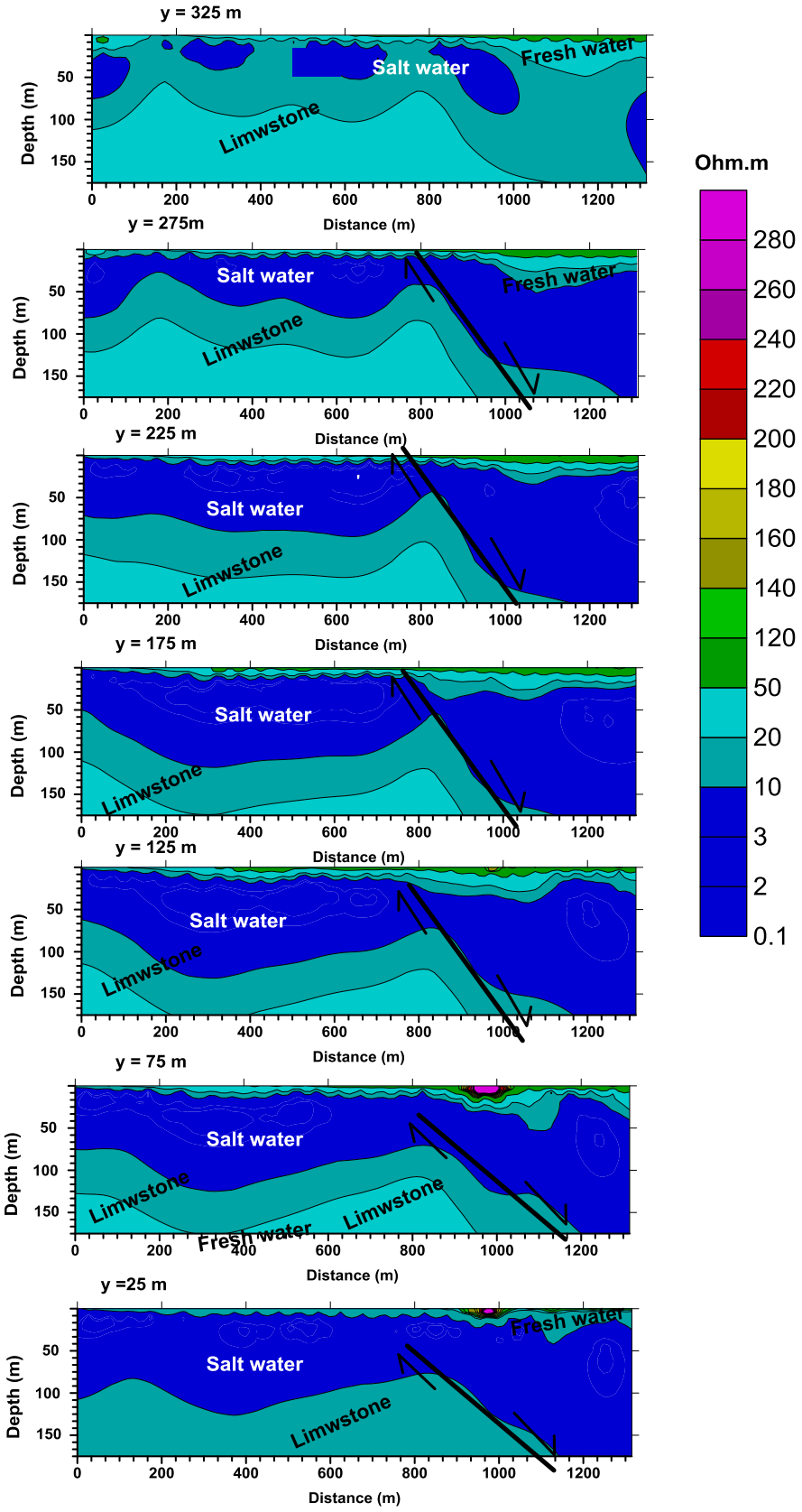

Figure 8 Vertical slices at *Y*-axis depths as a result of 3D VES inversion.

3.2. Shallow seismic refraction data

The shallow seismic refraction tool is the most commonly conducted geophysical technique for engineering investigations. Seismic refraction provides engineers and geologists with the most basic geologic data via simple procedures with the common equipment. Elastic body waves passing through homogeneous, isotropic media have well-defined equations of motion. Field surveys can readily yield wave velocities, V_P and V_S and for homogeneous, isotropic medium's engineering properties like Young's or elastic modulus (E) and shear modulus (G) and either density (ρ) or Poisson's ratio (σ) can be determined from V_P and V_S.

3.2.1. Shallow seismic data acquisition

In the present study, thirty-four shallow seismic refraction profiles (SP) have been carried out using a seismograph model StrataView of 48-channels manufactured by Geometrics; to cover the studied area. The length of every spread is 94 m (the length should be three to five times the maximum anticipated depth [25], using 48 vertical and horizontal geophones for measuring P-waves and S-waves with natural frequency of 40 Hz and geophones spacing of 2 m. A 25 kg hammer was used as the source of generated seismic waves. All seismic spreads have been carried out at the same locations of VES stations (Fig. 4). The aims of shallow seismic refraction survey are the identification of subsurface stratigraphy, subsurface structures and the calculation of geotechnical characteristics. The seismic refraction was carried out through applying the forward, mid-point and reverse acquisition system vertically and horizontally to create the compressional waves (P-waves) and shear waves (S-waves) which used in determining the seismic characteristic parameters.

3.2.2. Seismic data processing

It was pointed out that, the true refractor velocities can't be determined by shooting at only one end of a seismic line, but such velocities can be determined if the arrival times are recorded from both ends. Furthermore, a depth computed from an intercept time actually represents the depth of the refracting surface projected back to the shot point. The reversed profile, however, offers a significant advantage in that, the true velocities and thicknesses of layers can be computed beneath each. On the basis of the picking up of the first arrival of P-waves the wave forms are analyzed by picking the first arrivals using SIPT2 code (by Geometrics Company) and determining the travel time–distance (T-D) curves and depth models using both codes of SIPT2 and SeisRefa programs, which are complete seismic refraction processing and modeling software. These processes are based on the delay time and Hagiwara's method [26] for the determination of the specific depth for each refractor beneath each geophone along the spread.

3.2.3. Seismic data interpretation

According to the first arrival of P-waves and S-waves picking up, the wave forms are analyzed. The deduced time-distance curves and the corresponding 1-D depth model at each profile are obtained, in order to distinguish and interpret the subsurface layers and features as shown in Figs. 9 and 10. The results reveal that the subsurface layers consist of three layers in most of the seismic profiles. The velocity of the first upper layer ranges from 253 to 375 m/s corresponding to dry gravel and sand with a thickness of 0.5–1.5 m, second layer exhibits velocity ranging from 707 to 1152 m/s of sand and gravel with higher physical properties and its thickness ranging from 0 to 21.5 m. The third bottom layer reflects velocity ranging from 1445 to 2410 m/s corresponding to sandstone and shale.

3.2.4. Geo-seismic cross-sections

Four geo-seismic cross-sections have been constructed from the results of seismic spreads to indicate the variation in the lithology and structures which dissect the study area (Fig. 10). These geo-seismic sections indicate that the shallow part of the subsurface section consists of three layers, the first soil layer (dry gravels and sands of the recent deposits) is underlain by the second soil layer (sands and gravels of the Pleistocene) while the third layer is the bed rock layer (sandstones and shale of Middle Miocene). Also, the geo-seismic cross-sections exhibit a normal fault in the southeastern part of the study area with downthrown of the southeastern part.

3.3. Geotechnical characteristics

P-wave and S-wave velocities are used to compute the geotechnical characteristics (elastic moduli, competence scales and bearing capacities) of the detected third subsurface layer (bed layer).

3.3.1. Seismic velocities

In the seismic refraction method, the most important are the P-wave and S-wave energies. P-waves are the compressional body waves, where each particle moves in a direction collinear with the direction of propagation. S-wave energy also propagates as a body wave, through which the particle motion is transverse to the direction of travel of the wave. Seismic velocity is a function of the density (ρ) of the earth's material and the elastic properties (K) of that material. The velocity values of P-waves and S-waves are increased with depth where the velocity of P-waves is ranging from 253 to 375, 707 to 1152 and 1445 to 2410 m/s for the first, second and third layers (Fig. 11). The shear-wave velocities range from 159 to 243, 496 to 748 and 910 to 1217 m/s for the first, second and third layers respectively (Fig. 12).

3.3.2. Density

An empirical relationship given by [27] states that the increase in P-wave velocity with density has the following relation:

$$\rho = aV^{1/4} \quad (1)$$

where: ρ is the density, V is the P-wave velocity and a is a constant equal to 0.31, when the density is given in gm/cm^3 and velocity (V) is in m/s. In the study area, the density values range from 1.87 gm/cm^3 in the southeastern part to 2.18 gm/cm^3 in the northwestern part of the study area (Fig. 13a).

3.3.3. Poisson's ratio (σ)

Poisson's ratio (σ) is the ratio of lateral strain (perpendicular to an applied stress) to the longitudinal strain (parallel to applied stress). Poisson's ratio (σ) for the bed rock which is

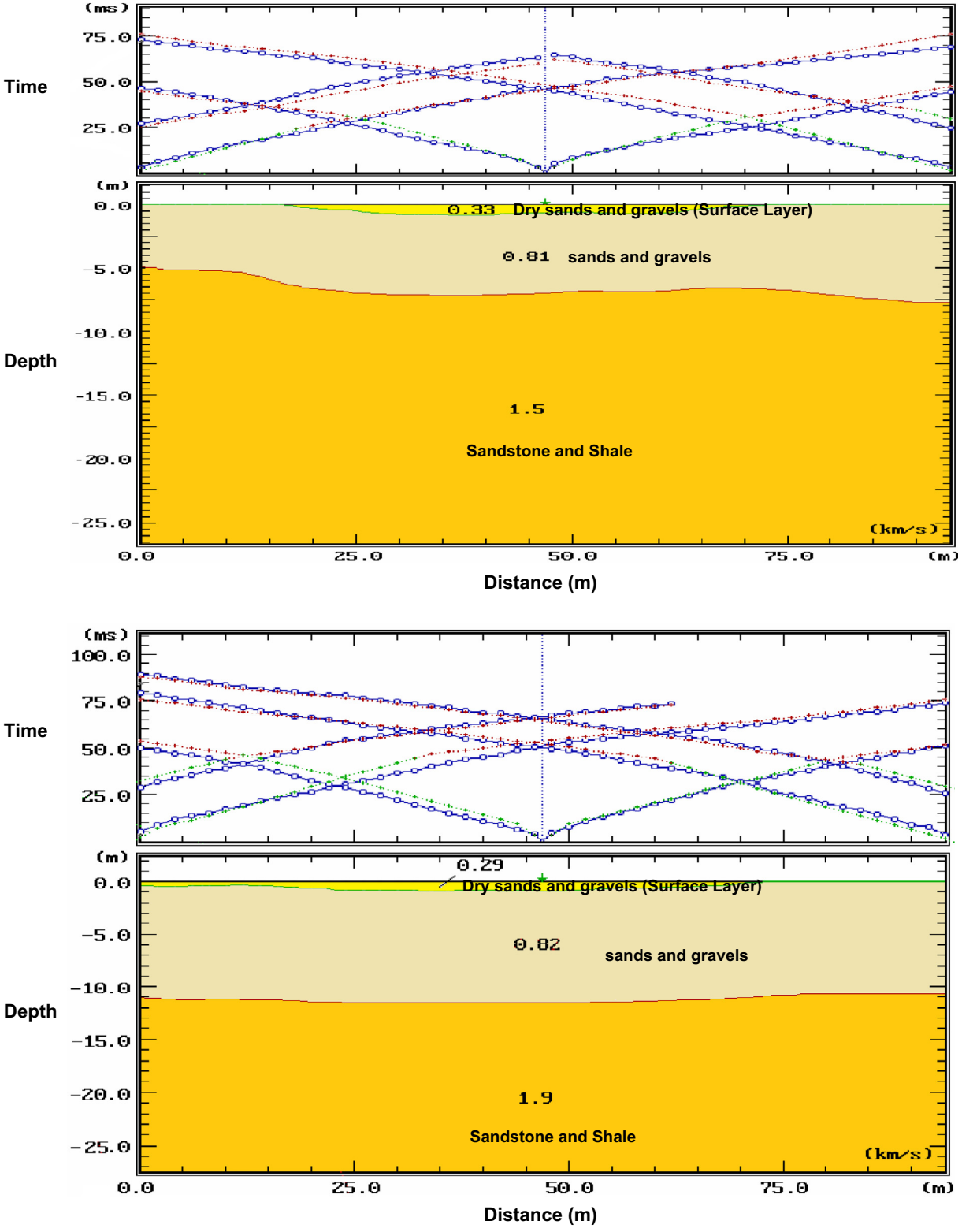

Figure 9 Time distance curve and depth model for seismic profile numbers 1 and 13.

composed of sandstone and shale of Middle Miocene (third layer) can be calculated from the following equation [28], where low competent rocks possess higher Poisson's ratio (σ) and vice versa.

$$\sigma = \frac{\left(\left(\frac{V_S^2}{V_P^2}\right) - \frac{1}{2}\right)}{\left(\left(\frac{V_S^2}{V_P^2}\right) - 1\right)} \quad (2)$$

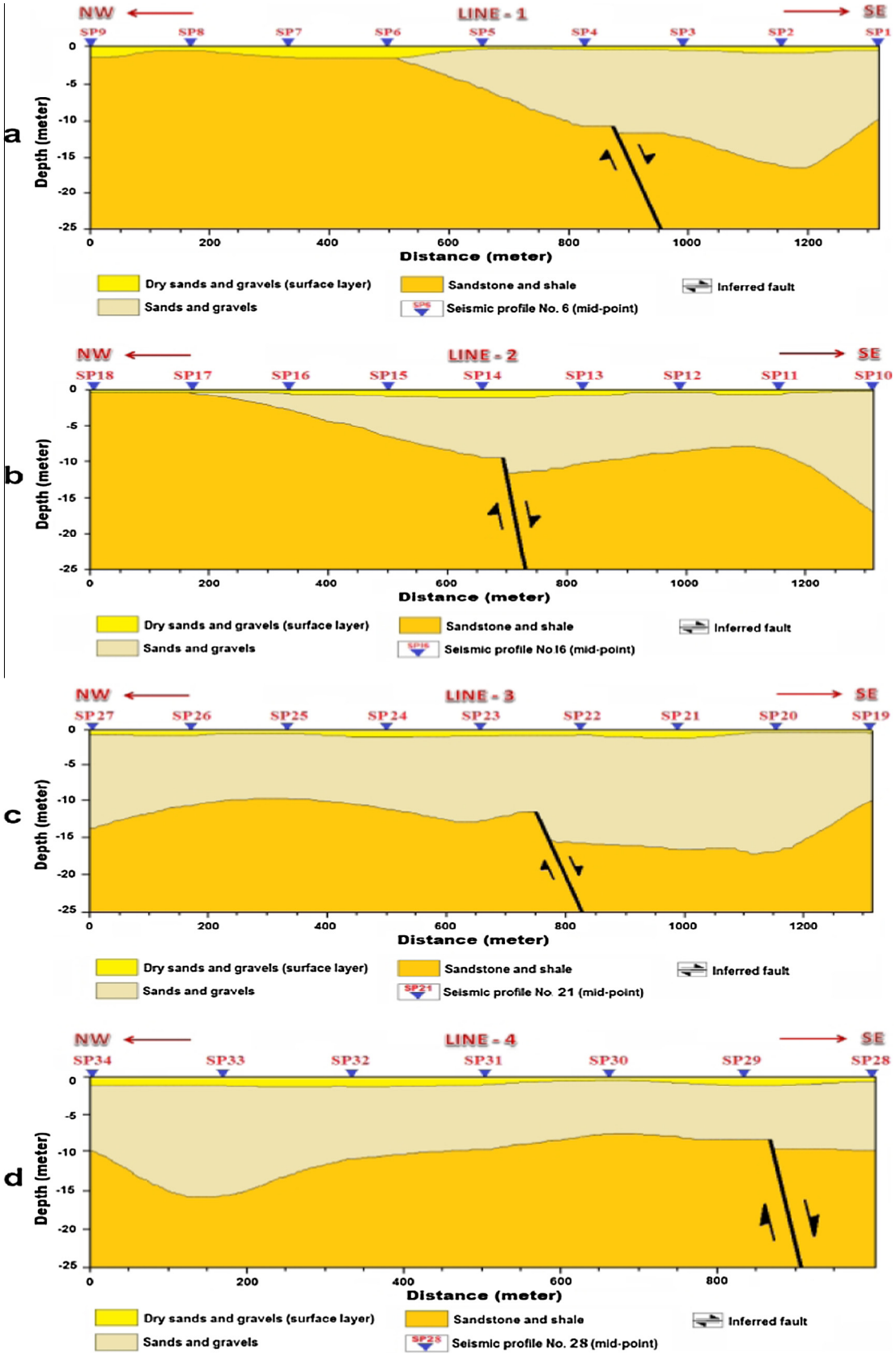

Figure 10 Geo-seismic cross-sections numbers 1, 2, 3 and 4 for a, b, c and d respectively.

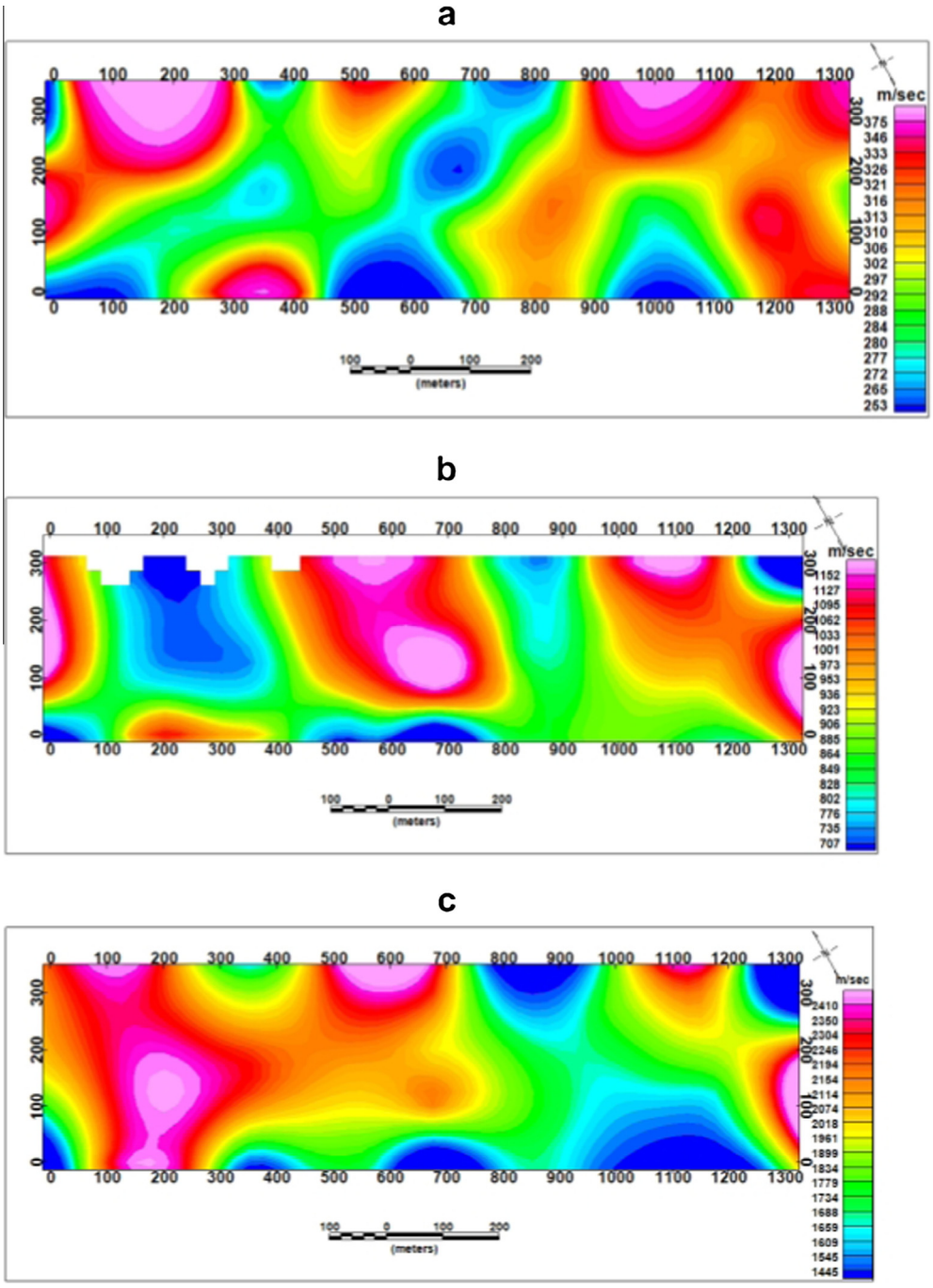

Figure 11 P-wave seismic velocities, (a) first layer, (b) second layer and (c) third layer.

In this study, the Poisson's ratio (σ) of the third layer (Fig. 13b) is high in most of the study area, specially in the northwestern part with values ranging from 0.24 to 0.357. These values reflects competent rock material, but in the south and southeastern parts low Poisson's ratio (σ) ranging from 0.167 to 0.24 is calculated, which reflects moderate competent rocks (Fig. 13b).

3.3.4. Elastic modulii

3.3.4.1. Rigidity modulus. The kinetic rigidity modulus (μ) is given in terms of shear wave velocity (V_S), density (ρ) and gravity acceleration (g) as follow:

$$\mu = V_S^2 \cdot \rho g \tag{3}$$

In the present study, the rigidity modulus (μ) exhibits values from 2.773×10^{10} dyn/cm^2 in the southern, northern and central parts to 9.2×10^{10} dyn/cm^3 in the northwestern part and southeastern parts of the study area (Fig. 14a).

3.3.4.2. Young's modulus (E). Young's modulus (E) is given in terms of rigidity modulus (μ) and Poisson's ratio (σ) as follows:

$$E = \mu(1 + \sigma) \tag{4}$$

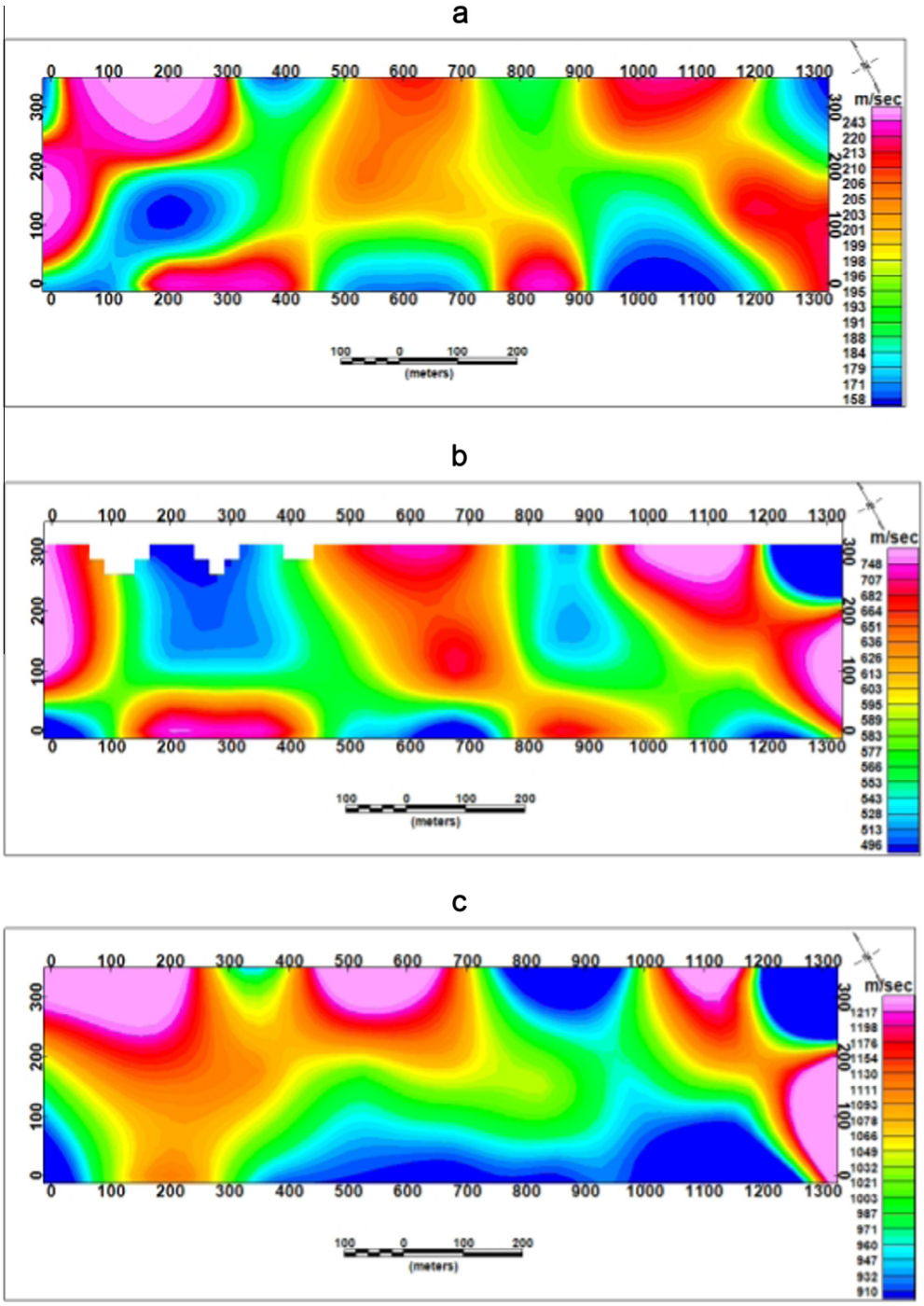

Figure 12 S-wave seismic velocities, (a) first layer, (b) second layer and (c) third layer.

The study area exhibits high Young's modulus in the northwestern and southeastern parts with values about 8.9163×10^{10} dyn/cm^2 but the southern, northern and central parts reflect low values about 0.9×10^{10} dyn/cm^2 (Fig. 14b).

3.3.4.3. Bulk modulus (K). The bulk's modulus (K) is given in terms of Young's modulus (E) and Poisson's ratio (σ) as follow:

$$K = E/(1 - 2\sigma) \quad (5)$$

The bulk's modulus (K) for the third layer (bedrock) characterized by values ranging from 1.23×10^{10} dyn/cm^2 in the southern, northern and central parts to 3.67×10^{10} dyn/cm^2 in the northwestern and southeastern parts of the study area (Fig. 14c).

3.3.5. Competence scales

3.3.5.1. Material index (Mi). Material index Mi is defined as the degree of competence of the material based on their elastic moduli. This index is related to the material composition, the

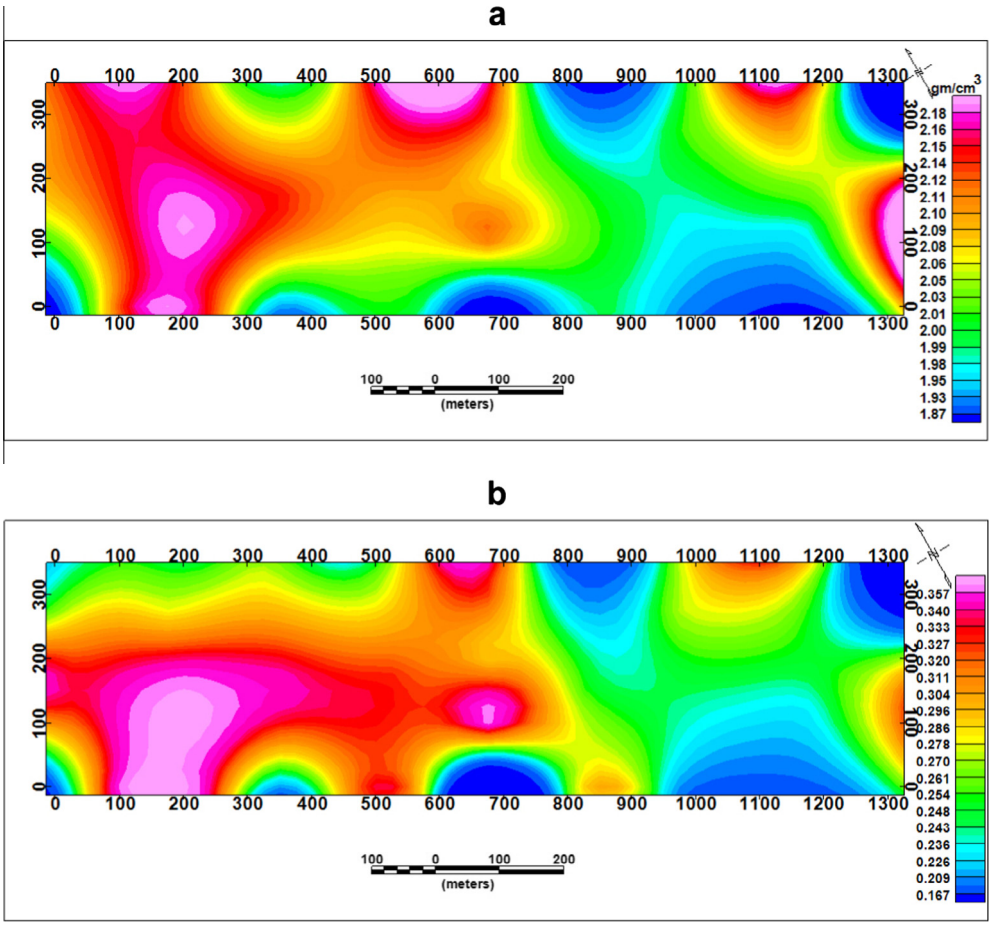

Figure 13 (a) density distribution map and (b) Poisson's ratio distribution map of the 3rd layer.

degree of consolidation, fracturing and jointing, the presence or absence of fluids in pore spaces, which affects the elastic moduli. The material index is given in terms of the elastic moduli [29] as follows:

$$\mathrm{Mi} = \frac{(\mu - \lambda)}{(\mu + \lambda)} = (1 - 4\sigma) \tag{6}$$

where: σ is Poisson's ratio and μ is the rigidity modulus. The distribution of material indices in the investigated area is determined in the third layer from the 34 seismic sites of the considered area as shown in Fig. 15a. This figure shows the material index distribution of the third layer where, the material index increases toward the northern, northeastern and southwestern parts.

3.3.5.2. Concentration index (Ci). The concentration index Ci describes the degree of material concentration. The soil compaction status is considered to a great extent as a measure of the degree of competence for foundation and other civil engineering purposes. It depends on both the elastic moduli of soil and the pressure distribution at their depths. The concentration index can be given in terms of velocity squared ratio [30] as:

$$\mathrm{Ci} = \frac{(3 - 4\alpha)}{(1 - 2\alpha)} \tag{7}$$

where: α is the velocity squared ratio $= \left(V_S^2/V_P^2\right)$. The concentration index is determined in the third layer for the 34 seismic sites of the concerned area as shown in Fig. 15b, which shows that the concentration index distribution of the third layer increases toward the northern, northeastern and southwestern parts and decreases throughout the remaining parts of the study area, as occurred for the other parameters.

3.3.5.3. Stress ratio (Si). The propagation velocity of seismic waves is proportional to the differential pressure between the sedimentary overburden and the pore filling fluids [30]. This means that, the high fluid pressure formations will have differential pressure and abnormally low seismic velocities. The stress ratio is expressed in terms of the velocity squared ratio as:

$$\mathrm{Si} = 1 - 2\left(V_S^2/V_P^2\right) \tag{8}$$

The stress ratio is determined for the third layer for the 34 seismic sites of the considered area as shown in Fig. 15c, which reflects increasing toward the northwestern and central parts of the study area.

3.3.5.4. Bearing capacities. The natural (earthquake) and the artificial (machine) cyclic dynamic loading create additional loads, which are added to the building load and may cause soil liquefaction, if the total loading value exceeds the ultimate

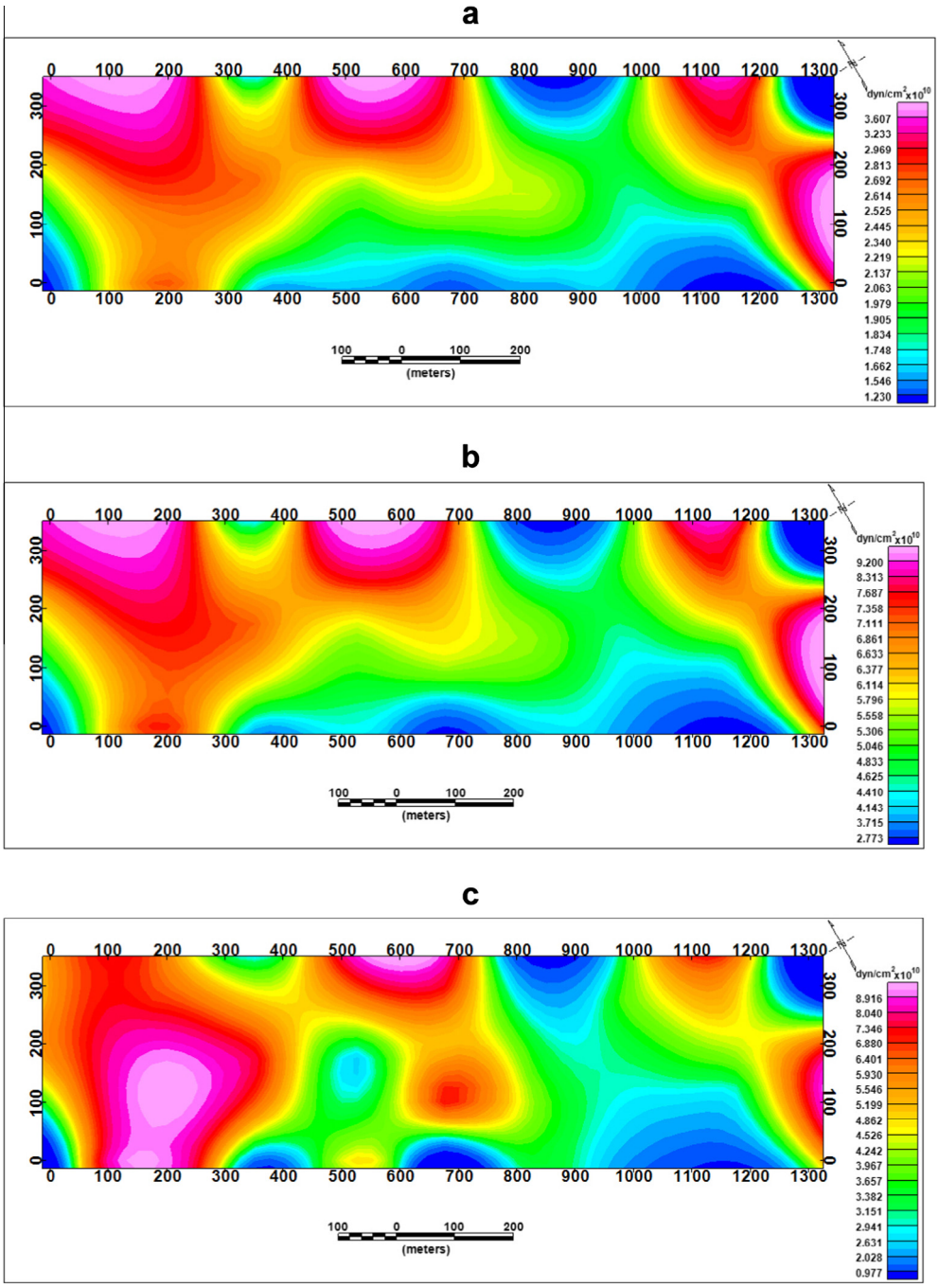

Figure 14 Elastic Moduli distribution maps of the third layer for (a) rigidity modulus (μ), (b) Young's modulus (E) and (c) bulk Modulus (K).

bearing capacity of the material [30]. The ultimate and allowable bearing capacities can be given in terms of shear-wave velocity [26] as:

$$\log Q_{ult} = 2.932(\log V_S - 1.45) \quad (9)$$

$$\log Q_{allow} = Q_{ult}/Fs \quad (10)$$

where: V_S is the shear-wave velocity, Q_{allow} is the allowable bearing capacity and Fs is the safety factor (ranges from 2 to 4). Both the ultimate and allowable bearing capacities are estimated in the third layer for the 34 seismic sites of the studied area, Fig. 16a and b where the ultimate and allowable bearing capacities are increased toward the northeastern, northern and southeastern parts of the study area.

4. Discussion

The integrated interpretation of geoelectric and shallow seismic data shows great compatibility over most parts of the study area. The interpretation of 3-D VES inversion indicates that the shallow subsurface section consists of gravel and sand, sand and shale saturated with fresh and salt water to depth of

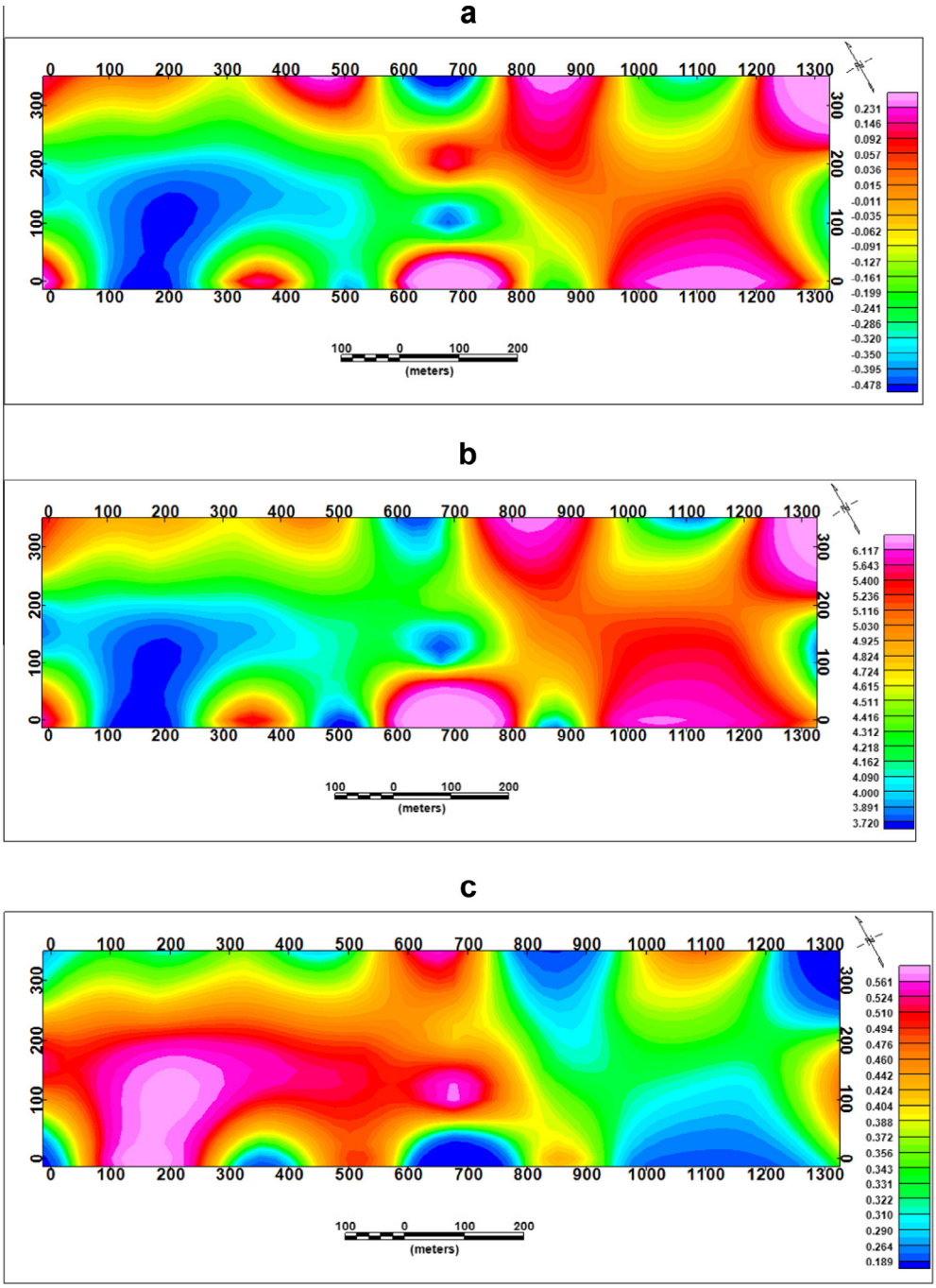

Figure 15 Material competence scales maps, (a) material index (γ), (b) concentration index (Ci) and (c) stress ratio (Si).

few meters in the northwestern part to about 20 m in the southeastern part. Also, the interpretation of shallow seismic data indicates that the northwestern part consists of soil (sand and gravel) of a few meters thickness overlaying the bed rock (sand and shale) while the southeastern part consists of thick soil layer about 10–20 m overlaying the bed rock (sand and shale). Both the interpretation of geoelectrical and shallow seismic data indicate that the study area is dissected by a normal fault crossing the southeastern part of the study area. The correlation between the interpretations of geoelectrical data is in compatibility with that of the data obtained from borehole drilled at distance of 2.5 km outside the study area. The subsurface section from the interpretation of both geoelectric and shallow seismic data are compatible with the geological sequence of the study area. The geotechnical characteristics from seismic interpretation indicates that the northwestern part of the study area exhibits more dense materials of high velocities and high competent at shallow depths.

Please cite this article in press as: S.A.S. Araffa et al., Geophysical investigation in the Northwestern part of the Gulf of Suez, Egypt, Egypt. J. Petrol. (2016), http://dx.doi.org/10.1016/j.ejpe.2016.06.002

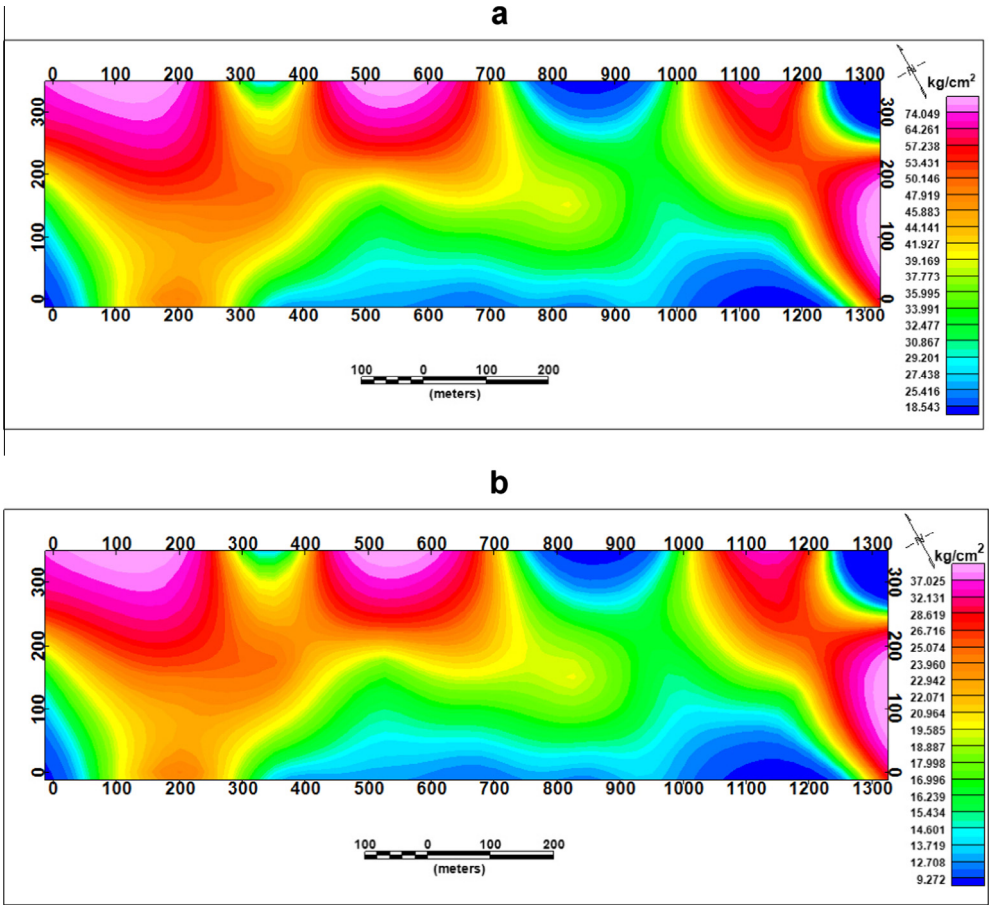

Figure 16 Foundation material bearing capacities, (a) ultimate bearing capacity (Q_{ult}) and (b) allowable bearing capacity (Q_{allow}).

5. Conclusion

From results of the interpretation of geoelectric and shallow seismic refraction data we can conclude that, the study area is composed of surface layer (soil) which consists of sand and gravels overlaying sand and shale layer. The sand and shale layer is saturated with fresh and salt water and overlaying a bedrock of limestone layer extend to a depth of 175 m. The depth of fresh water bearing zone ranging from a few meters in the northwestern part of the study area to about 25 m. The study area is dissected by a normal fault in the southeastern part of the study area. The northwestern part of the study area is suitable for any infrastructural purposes according to the results of the geotechnical characteristics obtained from seismic data.

References

[1] M.I. Youssef, M.A. Abdel-Rahman, in: 10th Arab Petroleum Conference, Tripoli, Libya, 135 (C-3), 1978, p. 8.
[2] M.N. EL-Ghamery, Geologic Development of the Cairo-Suez Area M.Sc. thesis, Fac. Sci., Al-Azhar Univ, 1985, p. 188.
[3] S.A.S. Araffa, B.S. Mohamed, in: Ann. Geol. Surv. Egypt V (XXIII) (2000) 901–918.
[4] W. Abou El-Saoud, Geoenvironmental Studies on New Cairo Area and Its Vicinity, Egypt, Using Remote Sensing Data and Geographic Information Systems M.Sc. thesis, Fac. Sci. Al-Azharuniv., 2006, p. 326.
[5] Hassaan, S.M., Abdeen, M.M., El Kazzaaz, Y.A., Yehia, M.A. and Attia, G.A., (2007) Characterization of the Oligocene sands and gravels, WadiGhoweiba, northwest Gulf of Suez, Egypt, using spectral signature and principle component analysis of terra Aster Image Egypt J. remote sensing and space sci., V. ll, pp. 73–92.
[6] S.M. Hassaan, Studying geological structures of Ayn-Sokhna area, north Eastern Desert, Egypt, by optimum utilization of data fusion techniques of some satellite image Ph.D. thesis, Fac. Sci. Helwan University, 2008, p. 207.
[7] A.M.E. Mohamed, A. Deif, S. El-Hadidy, S.S.R. Moustafa, A. El Werr, J. Geophys. Eng. 5 (2008) 420–437.
[8] A.M.E. Mohamed, J. Geophys. Prospect. 57 (2009) 1073–1089.
[9] J. Zhang, R.L. Mackie, T.R. Madden, Geophysics 60 (5) (1995) 1313–1325.
[10] S.K. Zhao, M.J. Yedlin, Geophysics 61 (1996) 1301–1307.
[11] M.H. Loke, R.D. Barker, Geophys. Prospect. 44 (1996) 499–523.
[12] P.I. Tsourlos, R.D. Ogilvy, J Balkan Geophys. Soc. 2 (2) (1999) 30–45.
[13] S.J. Yi Cho, S.H. Chung, J.H. Suh, Geophys. Prospect. 49 (2001) 483–497.
[14] A. Pidlisecky, E. Haber, R. Knight, Geophysics 72 (2) (2007) H1–H10, http://dx.doi.org/10.1190/1.2402499.
[15] M. Santos Fernando, S.A.S. Araffa, J. Appl. Geophys. 65 (2008) 97–110.
[16] S.A.S. Araffa, Int. J. Geophys. 192 (1) (2013) 94–112.
[17] A.M.E. Mohamed, S.A.S. Araffa, N.I. Mahmoud, Pure Appl. Geophys. 169 (2012) 1641–1654.
[18] S.A.S. Araffa, F.A. Monteiro Santos, T.A. Hamed, Environ. Earth Sci. 71 (2014) 3293–3305.

[19] EGSMA, (1999) Geotechnical study and groundwater exploration for the free economic area, Northwest Gulf of Suez, Egypt, internal report (in Arabic).
[20] A.M.E. Mohamed, Estimating Earthquake Ground Motions at the Northwestern Part of the Gulf of Suez, Egypt Ph.D. thesis, Ain Shams University, 2003 (Chapter 1).
[21] A.M. Abdallah, F.M. Abd El-Hady, U.A.R. J. Geol. 10 (1) (1966) 1–24.
[22] F.A. Monteiro Santos, A.R. Andrade Afonso, L.A. Mendes-Victor, J. Appl. Geophys. 37 (1997) 85–102.
[23] P. Represas, F.A. Monteiro Santos, A. Mateus, J. Figueiras, M. Barroso, R. Martins, V. Oliveira, M. Nolasco da Silva, J.X. Matos, Geophys. J. Int. 134 (2005) 736–746.
[24] Y. Sasaki, Geophysics 54 (1989) 254–262.
[25] B.B. Redpath, Seismic Refraction Exploration for Engineering Site Investigations, Technical Report E-73-4, U.S. Army Engineering Waterways Experiment Station Explosive Excavation Research Laboratory, Livermore, California, 1973.
[26] R.H.G. Parry, J. Geotech. Eng. Div. 103 (1977) 1014–1043.
[27] G.H.F. Gardner, L.W. Gardner, A.R. Gregory, Geophysics 39 (1974) 770–780.
[28] B. Sjögren, Shallow Refraction Seismics, Chapman & Hall., vii, London, New York, 1984, p. 270.
[29] M. Abdel-Rahman, Egypt J. Geol. 33 (1–2) (1989) 229–250.
[30] J.E. Bowles, Foundation Analysis and Design, 2nd Ed., Mc Graw-Hill International Book Company, London, 1984, p. 587.

Please cite this article in press as: S.A.S. Araffa et al., Geophysical investigation in the Northwestern part of the Gulf of Suez, Egypt, Egypt. J. Petrol. (2016), http://dx.doi.org/10.1016/j.ejpe.2016.06.002